A Model System for Photocatalysis: Ti-Doped α-$Fe_2O_3(1\bar{1}02)$ Single-Crystalline Films

Giada Franceschi,[1] Florian Kraushofer,[1] Matthias Meier,[1,2] Gareth S. Parkinson,[1] Michael Schmid,[1] Ulrike Diebold,[1] and Michele Riva[1,*]

[1]*Institute of Applied Physics, TU Wien, Wiedner Hauptstraße 8-10/E134, 1040 Wien, Austria*
[2]*Faculty of Physics and Center for Computational Materials Science, University of Vienna, Sensengasse 8, 1090 Wien, Austria*

Supporting Information

Description of Contents

S1. AS-GROWN FILMS

As mentioned in the main text, the growth conditions for our α-$(Fe_{1-x}Ti_x)_2O_3(1\bar{1}02)$ films (x = 0.0077, 0.0309), i.e., 850 °C and 2×10^{-2} mbar O_2, result in partial segregation of Ti to the surface. This is evident in XPS. Figure S1f shows the evolution of the Ti 2*p* peak of a 3.1 atom % film as a function of its thickness. The increase is not linear, suggesting that only part of the Ti segregates to the surface.

The surfaces of the as-grown films, both 0.8 atom % and 3.1 atom % (of 62 nm and 92 nm thickness, respectively) appear morphologically flat in the STM and AFM images shown in Figures S1a and S1d, respectively. Large parts of the surface of the 0.8 atom % film exhibit the well-known (1 × 1) structure of $Fe_2O_3(1\bar{1}02)$,[1] with dark rows that are identified as characteristic features induced by Ti doping in the main text. However, sparse, irregular patches with no evident periodicity coexist with these well-ordered regions (yellow arrow in Figure S1a). These patches feature roughly half the apparent height of a single step of the hematite surface (≈ 1.8 Å, to be compared with 3.68 Å for one O–Fe–O–Fe–O repeat unit). The disordered nature of these areas prevents us from performing fundamental studies at an atomic level, and motivated us to re-prepare the surface by Ar^+ sputtering plus UHV-compatible O_2 annealing (550 °C, 7×10^{-6} mbar). The resulting surface, shown in Figure S1b and Figure 2b (main text), is an almost perfect $Fe_2O_3(1\bar{1}02)$-(1 × 1).

The surface of the as-grown 3.1 atom % film was not measured in STM right after growth. The *ex-situ* AFM image in Figure S1d reveals the presence of round-shaped, 10–40 nm-wide features, never observed on UHV-treated hematite surfaces. Both the unusual appearance of the surface and the ≈ 6.2-fold higher XPS Ti 2*p* signal with respect to the 0.8 atom %-doped film (values extracted from the spectra in Figure S1c,f) suggest that a new, Ti-rich phase formed at the surface. The Ti XPS increases more than in proportion to the doping level. A possible explanation is that this new phase, once nucleated, catches deposited Ti and floats up during growth. We consider it likely that the formation of this Ti-rich phase is related to the rather high oxygen pressures used (PLD growth was performed at 2×10^{-2} mbar O_2), while it is not favorable under more reducing conditions. This may be related to the fact that substitutional Ti^{4+} in the Fe_2O_3 lattice leads to Fe^{2+}, while higher oxygen chemical potentials favor Fe^{3+}, which can coexist with Ti^{4+} only in a different crystal lattice such as in Fe_2TiO_5 (pseudobrookite). Similarly to the low-doped film, we investigated this higher bulk doping on a UHV-prepared surface rather than on the as-grown film. After two sputtering–annealing cycles, the Ti 2*p* spectra saturate to the one shown in Figure S1f with red symbols. In STM, the surfaces appear as in Figure S1e and Figure 2c (main text), i.e., an $Fe_2O_3(1\bar{1}02)$-(1 × 1) with dark rows (with a density 4.57 ± 0.60 times larger than on the 0.8 atom % doped film, see main text). These results show that, despite the accumulation of Ti in the near-surface region that is caused by Ti segregation during growth, we can recover well-defined hematite surfaces that are only slightly modified by the presence of Ti.

* Corresponding author: riva@iap.tuwien.ac.at

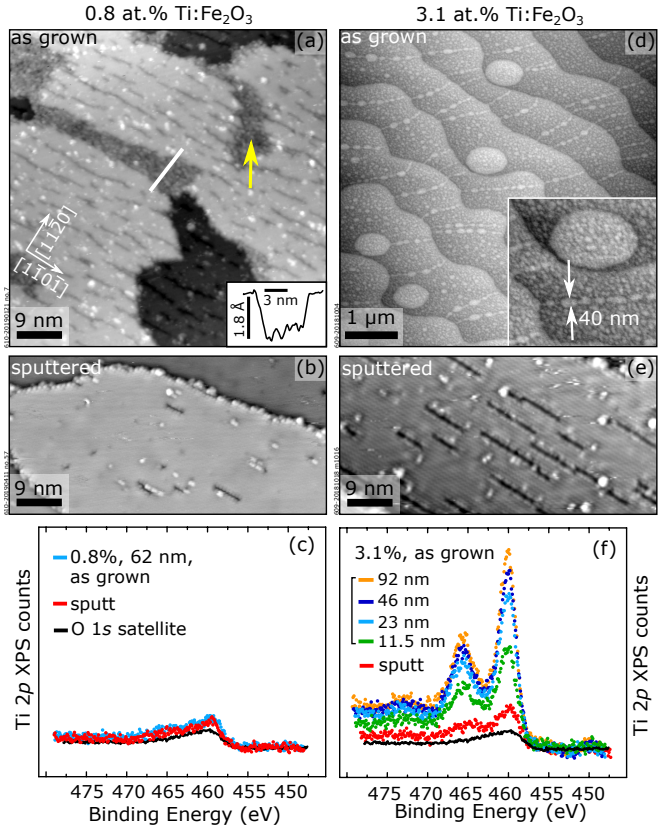

Figure S1. Segregation of the Ti dopants during the PLD growth of Ti:$Fe_2O_3(1\bar{1}02)$ films. (a) and (b) STM images of a 0.8 atom % Ti-doped film of 62 nm thickness right after growth, and after UHV preparation, respectively. After growth, disordered areas, presumably Ti-rich phases [yellow arrow in (a), line profile along the white line in the inset] coexist with (1 × 1) areas with dark rows. (b) After one sputtering–annealing cycle, a mostly (1 × 1) surface is recovered. (c) The corresponding XPS Ti 2*p* signals are only slightly above the detection limit, thus it is difficult to determine whether the surface Ti concentration decreases with sputtering. (d) 6 × 6 µm² AFM image of a 3.1 atom % Ti-doped film of 92 nm thickness after growth, showing bright, circular features on the terraces. (e) After sputtering, the surface displays a (1×1) periodicity with dark rows in STM. (f) XPS of the as-grown film shows significant Ti enrichment, which increases with thickness, but is efficiently removed by sputtering.

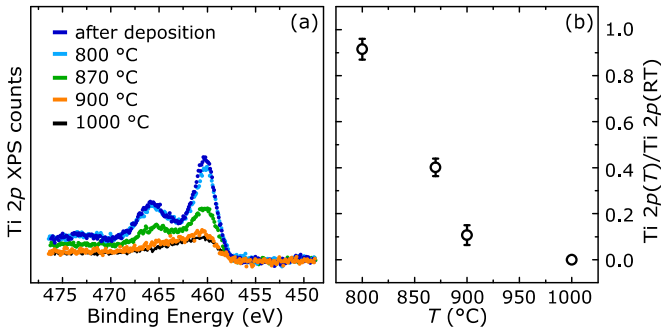

Figure S2. (a) XPS Ti 2*p* spectra measured on a UHV-prepared, undoped α-$Fe_2O_3(1\bar{1}02)$ single crystal after depositing 0.32 ML Ti at room temperature and annealing for 15 min at the temperatures indicated (the sample was reprepared each time). The scale of the vertical axis is the same as in Figure S1c,d. Increasing temperatures cause Ti diffusion toward the bulk until the pristine sample is recovered at 1000 °C (the peak in the black curve is associated to the O 1*s* satellite due to Al $K\beta$ emission). (b) Intensity of peaks from panel (a), normalized to the intensity measured after each corresponding deposition at room temperature.

S2. CHOICE OF DEPOSITION TEMPERATURE

The substrate temperature is a critical parameter for the growth of high-quality films. High temperatures are generally needed to obtain good crystallographic order and morphology. At the same time, they can be detrimental in the presence of dopants: High temperatures might cause irreversible migration of the dopants into the bulk of the substrate, or their segregation to the surface. While it has been reported both experimentally and computationally[2,3] that Ti atoms substitute Fe cations in the bulk of doped films in a random fashion, it has been also observed that Ti tends to accumulate at the hematite surface.[4] For this reason, when the growth is realized from a mixed target, lower temperatures are to be preferred. In our case, however, we introduce the doping by alternating growth from TiO_2 and Fe_3O_4 targets. As a result, one needs to find an appropriate temperature that allows sufficient diffusion of the Ti dopants and achieve a reasonably uniform doping profile, while avoiding major segregation and/or irreversible migration into the bulk. From a practical point of view, an even distribution of dopants is desirable for providing an effective electrical contact between the film and the Pt electrodes.

We tested the behavior of Ti dopants with the annealing temperature. We deposited a fixed amount of Ti in PLD: 10 laser pulses [or 0.32 ML, where 1 ML corresponds to two atoms per (1 × 1) surface unit cell, or 7.3×10^{14} at./cm²] at room temperature, and 2×10^{-2} mbar O_2 on a UHV-prepared, undoped $Fe_2O_3(1\bar{1}02)$ single crystal. We then annealed the sample for 15 min at increasingly higher temperatures at 2×10^{-2} mbar O_2. The deposited amount was chosen small enough to avoid the formation of ill-defined, Ti-rich areas [it causes the formation of dark rows on an otherwise unchanged hematite (1 × 1) surface], but sufficiently large to provide an XPS Ti 2*p* signal with good signal-to-noise ratio. To ensure deposition of consistent amounts of material in all experiments, the O_2 pressure was kept constant during deposition. The sample was reprepared by annealing for 30 min at 1000 °C, 0.2 mbar O_2 before each deposition/annealing experiment (these parameters allow all Ti to irreversibly diffuse in the bulk). The corresponding XPS Ti 2*p* spectra are shown in Figure S2a. Figure S2b shows their intensity, normalized to the intensity of the peak after room-temperature deposition, plotted against the annealing temperature. The almost unchanged

signal observed upon annealing at 800 °C suggests that dopant diffusion is largely inhibited at this temperature. On the other hand, annealing at 870 °C and 900 °C leads to a decrease of the XPS signal by 60% and 90%, respectively, while at 1000 °C the Ti signal is completely lost. These results are consistent with literature data on iron self-diffusion in bulk hematite single crystals[5–7] (while no data exist for bulk diffusivity of Ti dopants in hematite, one can expect diffusion coefficients of Ti to be comparable to those of Fe). From the diffusion constants estimated there, at 800 °C, Fe cations are to travel only $0.1 - 0.3$ nm in 15 min. At higher temperatures they can cover longer distances ($0.7 - 3$ nm at 900 °C, and $4 - 24$ nm at 1000 °C), consistent with the observed decrease of the XPS intensity. These findings can also explain the saturation of the coverage of dark lines after annealing for 10 min at 550 °C (Figure 4): The concentration of subsurface Ti remains unchanged because bulk diffusion is inhibited at this temperature (in the bulk, the diffusion length of Fe cations would be 10^{-4} nm in 40 min at 550 °C).

We therefore chose a growth temperature of 850 °C because it allows step-flow growth and fast dopant diffusion while avoiding complete (irreversible) diffusion into the bulk of the substrate. Post-growth tests performed on our films grown at 850 °C, 2×10^{-2} mbar O_2 support this choice: First and foremost, the samples are sufficiently conductive to study them by STM at room temperature ($U_{\text{sample}} = +2$ V, $I_t = 0.2$ nA) after a single sputtering–annealing cycle, as opposed to undoped single crystals, which typically require reduction of the bulk via tens of cycles.[1] Moreover, the coverage of dark rows at the surface, directly correlated to the amount of subsurface Ti (see main text), stays roughly unchanged upon performing several consecutive sputtering–annealing cycles. This suggests a reasonably uniform distribution of the dopants within the films.

S3. DETERMINATION OF BULK DOPING

The bulk doping level in Ti:$Fe_2O_3(1\bar{1}02)$ films grown by PLD from two different targets cannot be trivially determined by the ratio of laser pulses shot on the iron-oxide and on the titania targets. Different absorption of the UV laser, sticking effects, as well as the specific values of the oxygen chemical potential and the laser fluence, can affect the distinct species differently.[8,9] To determine the doping level in our films, we separately evaluated the amounts of Fe and Ti deposited per pulse. We then translated this information in the relative number of shots on the two targets needed for a specific doping level.

The technique of choice for quantifying these submonolayer amounts was STM. While XPS could in principle be used for the same purpose, it is more demanding, as it requires (i) modeling the dopant distribution, (ii) knowing the relative sensitivity factors for Fe and Ti, and (iii) ensuring that photoelectron diffraction effects on our single-crystalline samples do not alter the Ti and Fe intensities. A reliable evaluation of the Ti amount deposited per pulse requires to precisely measure amounts around 0.1 ML. If larger amounts are deposited at once (around 1 ML), Ti-rich phases form, which can complicate the quantification.

Amount of Ti deposited per pulse. Since a conductive sample is required to perform STM, we started with a "low-doped" film with an almost perfect (1×1) termination, as per Figure 2b. To ensure that the same amount of ablated material was reaching the substrate, we deposited Ti at the same laser fluence and oxygen pressure (2.0 J/cm^2, 2×10^{-2} mbar O_2) as during growth. However, we used a lower sample temperature (550 °C) to avoid segregation/interdiffusion of Ti. While the lower temperature might lead to a slight overestimation of the amount deposited due to a possibly larger sticking at 550 °C versus 850 °C, the very low vapor pressure of Ti species (for Ti metal: 4×10^{-12} mbar at 850 °C, and $\approx 5 \times 10^{-20}$ mbar at 550 °C; possibly even lower for Ti–O species) suggests that re-evaporation can be neglected. We quantified the amount of Ti deposited per pulse by evaluating the coverage of dark rows that thereby developed, using the estimated number of Ti atoms per unit cell that yield the dark rows, as inferred from our DFT results (see main text). Our reference is the trench structure with (2×1) periodicity (Figure S4), which is characterized by 50% coverage of dark rows, and corresponds to one Ti atom per (1×1) surface unit cell, i.e., 0.5 ML Ti. As a baseline, we first evaluated the coverage of dark rows on the pristine sample that was annealed for one minute at the same conditions later used for the deposition. This reference number was subtracted from subsequent evaluations. We repeated the same experiment by depositing first one pulse of TiO_2, then three pulses, each time repreparing the sample in between and keeping the annealing time within one minute. The two experiments gave consistent results, and showed that a single laser pulse causes an increase of the trench coverage of 3.2%, corresponding to $T_{\text{Ti}} = 3.2 \times 10^{-2}$ ML per pulse.

Amount of Fe deposited per pulse. Since our growth mode is step flow, it is not possible to evaluate the amount of Fe deposited per pulse from the RHEED oscillations typically present in layer-by-layer mode. We measured the thickness of a Ti-doped film grown with a known number of pulses with a stylus profilometer. We found that 60 000 Fe pulses with 120 intervening Ti pulses, deposited at 850 °C, 2×10^{-2} mbar O_2, 2.0 J/cm^2, correspond to a thickness of (91.5 ± 7.4) nm, or $T_{\text{tot}} = (497 \pm 40)$ ML (given an interlayer spacing of 0.368 nm/bilayer, and that one bilayer of hematite contains four cations per unit cell, or 2 ML). We can then derive the amount of Fe atoms deposited per pulse as $T_{\text{Fe}} = (T_{\text{tot}} - 120T_{\text{Ti}})/60000 = (8.22 \pm 0.67) \times 10^{-3}$ ML.

Estimation of the doping level. With the evaluation of the amount of Ti and Fe deposited per pulse in units of monolayer, and knowing the relative number of pulses shot

on the two targets during growth, we can estimate the doping level. The low-doped film has a 1:500 ratio of laser pulses on the TiO_2:Fe_3O_4 targets; hence, the doping level can be evaluated as $(1 \times T_{Ti})/(1 \times T_{Ti} + 500 \times T_{Fe}) = (0.77 \pm 0.06)$ atom %. The highly doped film, with a fourfold higher ratio (3:375), has then a (3.09 ± 0.24) atom % doping level. To simplify the reading, we refer to these doping levels as 0.8 atom % and 3.1 atom %, respectively. We should mention that part of the deposited Ti segregating during growth is removed by the UHV treatments, especially for the 3.1 atom %-doped film (see Figure S1f). As a result, the true doping level of the bulk will likely be marginally smaller than 3.1 atom %. However, quantifying the amount of Ti removed by these treatments from XPS data is not trivial because the distribution of dopants at the surface of the as-grown film is unknown.

S4. ESTIMATION OF THE DISCREPANCY BETWEEN DFT AND EXPERIMENTAL μ_O

We expect the largest difference between μ_O^{DFT} and μ_O^{exp} (both defined in Section 2 of the main text) to arise from the absence of entropic (vibrational) terms in the definition of $\mu_O^{DFT} = E_{O_2}/2$ in place of $\mu_O^{DFT} = (H_{O_2} - TS_{O_2})/2$. This is a common assumption when dealing with *ab-initio* thermodynamics that can lead to errors in μ_O^{DFT} of the order of a few hundred millielectronvolts.[10] A possible way to roughly estimate the error introduced by disregarding entropic terms is determining the value of the oxygen chemical potential $\mu_O^{Fe_2O_3 \rightleftharpoons Fe_3O_4} = 3E_{Fe_2O_3} - 2E_{Fe_3O_4}$ at which Fe_2O_3 is reduced to Fe_3O_4, as determined from the equilibrium reaction

$$3\,Fe_2O_3 \rightleftharpoons 2\,Fe_3O_4 + \frac{1}{2}O_2\,.$$

To this aim, we have also calculated the DFT energy, $E_{Fe_3O_4}$, of Fe_3O_4 with the same computational setup, resulting in $\mu_O^{Fe_2O_3 \rightleftharpoons Fe_3O_4} = -2.46$ eV. This can be compared to the value $\mu_O^{Fe_2O_3 \rightleftharpoons Fe_3O_4} \approx -2.15$ eV obtained at 550 °C (i.e., the temperature used in our experiments) from the phase diagram of iron oxides.[11] This difference would shift the transition thresholds between the $(1 \times 1)_{Ti}$ and the trench structure predicted by DFT by ~ 0.3 eV toward larger chemical potentials. Notice, however, that this estimate necessarily includes a combination of possible errors in the determination of the DFT energies for Fe_2O_3 and Fe_3O_4. It is not clear to which extent these DFT errors cancel each other out, and, consequently, how accurate the estimate can be considered. For example, possible DFT errors related to the different coordination of Fe in hematite (octahedral only) and magnetite (both octahedral and tetrahedral) do enter the estimate above, but should largely cancel out when comparing our structures (all Fe atoms are octahedrally coordinated).

S5. DENSITY OF STATES OF THE TRENCH STRUCTURE

Figure S3a shows the density of states (DOS) for selected atoms of an infinite trench structure with $U_{eff} = 4$ eV. A (6 × 1) cell with two Fe atoms of layer C2 substituted by Ti was used in this case, as represented in Figure S3b. The DOS is shown for Ti (blue) and for selected iron and oxygen atoms occupying bulk-like sites (gray), and surface sites both far away (green) and at the edge of the Ti-induced trench (red). The DOS for surface atoms inside the trench is qualitatively similar to the one for atoms at the trench edge.

With $U_{eff} = 4$ eV, the electronic band gap of bulk-like atoms amounts to ~ 1.8 eV. This value is at the lower end of the range of experimentally reported band gaps.[12] The Ti dopants, as well as the Fe and O atoms close to the trench (red curve) exhibit an additional in-gap state slightly above the valence band maximum. Conversely, an increased density of states ~ 0.5 eV below the valence band maximum is visible for surface Fe and O atoms far from the surface defect (green, highlighted with a star in Figure S3a). In addition, part of the empty *d* states of these Fe atoms is concentrated in a sharp peak at approximately +2.1 eV (also indicated with a star). These Ti-induced modifications of the local density of states might explain the larger apparent height of atoms far away from trenches observed in STM with respect to those closer to the trench (Figure 7 of the main text).

To assess the effect of our choice of U_{eff}, we also performed density-of-states calculations with modified U_{eff} for this structure. Keeping $U_{eff}^{Fe} = 4$ eV for Fe and using $U_{eff}^{Ti} = 5$ eV for the Ti dopants does not change the band gap of bulk-like Fe atoms, but increases the density of the in-gap state and weakens the accumulation of states at the valence band edge for surface Fe and O atoms far from the trench. Using $U_{eff} = 5$ eV for both Fe and Ti atoms similarly modifies in-gap states and conduction band edge (though to a smaller extent). In addition, the band gap widens to ~ 2.0 eV, reaching values closer to the those reported experimentally.[12] None of these quantitative modifications to the DOS results in major qualitative differences in the existence or distribution of electronic states.

S6. RELATION BETWEEN SURFACE DOPING, COVERAGE OF TRENCHES, AND TITANIUM COVERAGE

Consistent with the established definition of bulk doping in atomic percent, we defined in the main text the "surface" doping as $c_{Ti}^s = n_{Ti}/(n_{Ti} + n_{Fe})$, where n_{Ti} and n_{Fe} are the numbers of Ti and Fe cations in layers C1 and C2. In light of the DFT models of the trench structures, one can relate the coverage of trenches θ measured by STM and the surface doping defined above. In this section, we derive this relation explicitly.

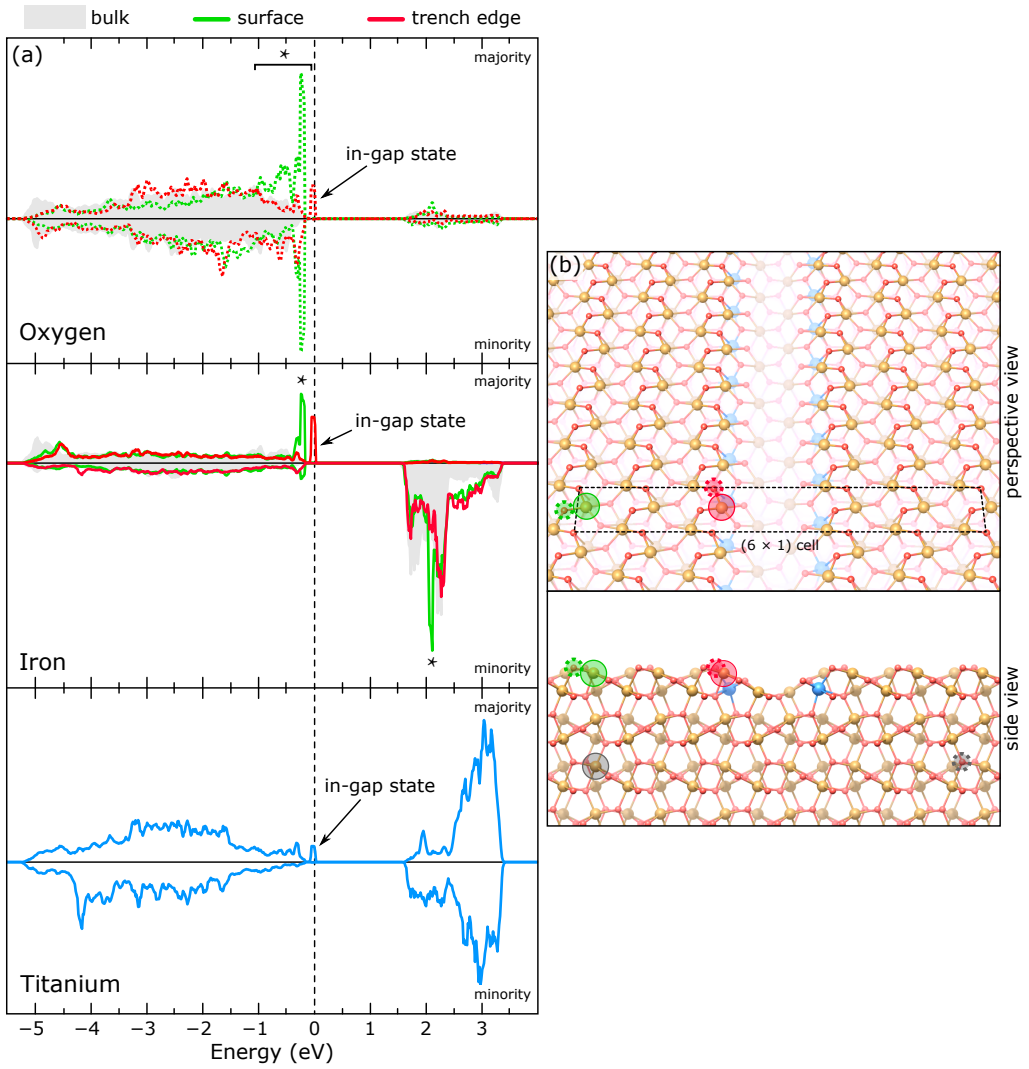

Figure S3. Density of states for atoms in an infinite trench structure. (a) DOS for selected O (top), Fe (middle), and Ti atoms (bottom). In the top and middle panels, the DOS of bulk-like Fe and O atoms is plotted as a solid, gray region, while curves correspond to surface atoms far away (green), and at the edge of the trench (red). The corresponding Fe and O atoms are highlighted in the structural model of panel (b). The calculation was performed on a (6 × 1) cell with two Fe atoms substituted by Ti in layer C2, and $U_{\text{eff}} = 4$ eV. In panel (a), the Fermi level (dashed vertical line) is set such that the total number of occupied states equals the number of electrons in the slab. In panel (b), Fe, O, and Ti atoms are depicted as yellow, red, and blue spheres, respectively.

As shown in the main text, a trench is formed as a result of the substitution of 2 Fe atoms in layer C2 by 2 Ti atoms in a (2 × 1) cell, and the simultaneous removal of 2 additional Fe atoms from layer C1 in the same cell (refer to the structural models in Figure 6). We measure θ as the fraction of Fe atoms removed from layer C1 when a trench is formed: 2 Fe atoms removed from layer C1 in a (2 × 1) cell (that contains four atoms), corresponds to a 50% coverage of trenches (i.e., the structure in Figure 6c), or $\theta = 0.5$ ML.

Consider now that each cation layer in a (1 × 1) cell of undoped $Fe_2O_3(1\bar{1}02)$ contains two atoms. Doping an ($l \times m$) cell with k Ti atoms results in (i) replacement of k Fe atoms in layer C2 (out of the $2lm$ originally present), and (ii) removal of k Fe atoms from layer C1 (out of the $2lm$ originally present). Thus, the coverage of trenches amounts in this case to $\theta = k/(2lm)$, while the doping is

$$c^{\text{s}}_{\text{Ti}} = \frac{n_{\text{Ti}}}{n_{\text{Ti}} + n_{\text{Fe}}} = \frac{k}{k + 2 \times (2lm - k)} = \frac{k/(2lm)}{2 - k/(2lm)} = \frac{\theta}{2 - \theta}\,.$$

Following our definition of monolayer, the coverage of Ti is, instead, the fraction of cations in layer C2 replaced by Ti, i.e.,

$$\theta_{\text{Ti}} = \frac{k}{2lm} = \theta\,.$$

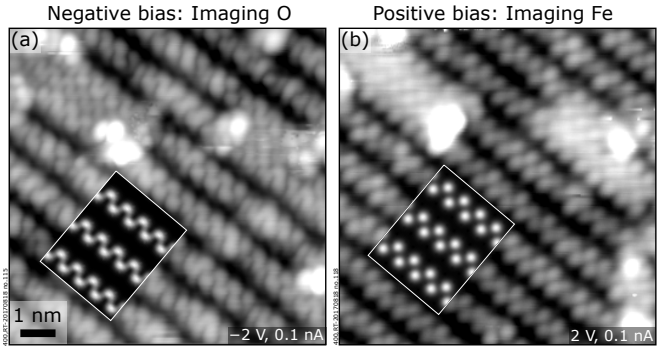

Figure S4. Experimental (main panels) and simulated (insets) STM images of the $Fe_2O_3(1\bar{1}02)$-trench reconstruction with a (2 × 1) periodicity, obtained by depositing 0.5 ML Ti at room temperature on an undoped $Fe_2O_3(1\bar{1}02)$-(1 × 1) surface, followed by 20 min annealing in UHV at 600 °C, plus depositing another 0.5 ML Ti at room temperature followed by 30 min annealing at 1×10^{-6} mbar O_2 and 550 °C [similar results were obtained after the deposition of the first 0.5 ML Ti, that are sufficient to form the trench reconstruction with (2×1) periodicity]. The experimental images are 9×9 nm^2. The STM simulations (shown in overlay) are based on the trench model of Figures 5c and 6c, and were performed at constant height (3.3 Å above the surface), with $U_{\text{sample}} = -1$ V, +2 V in (a) and (b), respectively.

S7. FULL COVERAGE OF THE TRENCH STRUCTURE

As discussed in the main text, the near-surface Ti present in our doped films causes the formation of isolated and short trench defects. However, for most chemical potentials, DFT predicts the most favorable configuration as a full (2 × 1)-periodic ordering of the Ti-induced trenches, as per Figure 5c of the main text. This configuration is not realized on our films because the amount of near-surface Ti is too low. However, it can be obtained by depositing large amounts of Ti (> 0.5 ML) on an $Fe_2O_3(1\bar{1}02)$-(1×1) surface followed by oxygen annealing. Figure S4 shows STM images of an undoped $Fe_2O_3(1\bar{1}02)$-(1 × 1) surface after deposition of 1 ML Ti followed by oxygen annealing at 550 °C and 1×10^{-6} mbar. Comparable results were obtained after deposition of only 0.5 ML Ti followed by annealing at the same conditions. The resulting structure is imaged as zigzag lines with a (2 × 1) ordering at both positive and negative sample bias. The STM simulations, shown as overlay, are in good agreement with the experimental images. At negative sample bias (probing filled states), the visible zigzag rows correspond to oxygen; every other zigzag row is missing due to the (2 × 1) trenches. At positive sample bias (probing empty states), Fe is imaged; here, half of every zigzag of the original (1 × 1) structure is missing, and every zigzag line imaged on the (2 × 1) structure consists of the remaining halves of two (1 × 1) zigzag lines. This new zigzag visible on the (2 × 1) structure essentially corresponds to the rows of single protrusions lining the edges of a trench for isolated trench defects (see Figure 7b of the main text), paired with the same features in the neighboring trench. It is worth noting that, based on the structural model, 0.5 ML Ti should be sufficient to saturate the trench structure with a (2 × 1) periodicity; however, there is no sign of excess Ti in the STM images in Figure S4, suggesting that additional Ti substitution in the subsurface does not cause further changes to the surface structure at these coverages. (Diffusion of Ti into the deep bulk should be inhibited at the temperature used in this preparation, see Section S2.)

S8. NAMING CONVENTION FOR STRUCTURAL (.CIF) FILES

We include .cif files for selected structures. The file names are composed as follows:

FigureNumber - DFTCellSize - N_{Ti} - descriptive name

[1] F. Kraushofer, Z. Jakub, M. Bichler, J. Hulva, P. Drmota, M. Weinold, M. Schmid, M. Setvin, U. Diebold, P. Blaha, and G. S. Parkinson, Atomic-scale structure of the hematite α-$Fe_2O_3(1\bar{1}02)$ "R-cut" surface, J. Phys. Chem. C. **122**, 1657 (2018).

[2] H. Magnan, D. Stanescu, M. Rioult, E. Fonda, and A. Barbier, Enhanced photoanode properties of epitaxial Ti doped α-$Fe_2O_3(0001)$ thin films, Appl. Phys. Lett. **101**, 133908 (2012).

[3] T. Droubay, K. M. Rosso, S. M. Heald, D. E. McCready, C. M. Wang, and S. A. Chambers, Structure, magnetism, and conductivity in epitaxial Ti-doped α-Fe_2O_3 hematite: Experiment and density functional theory calculations, Phys. Rev. B **75**, 104412 (2007).

[4] J. A. Glasscock, P. R. F. Barnes, I. C. Plumb, and N. Savvides, Enhancement of photoelectrochemical hydrogen production from hematite thin films by the introduction of Ti and Si, J. Phys. Chem. C **111**, 16477 (2007).

[5] A. C. S. Sabioni, A. M. Huntz, A. M. J. M. Daniel, and W. A. A. Macedo, Measurement of iron self-diffusion in hematite single crystals by secondary ion-mass spectrometry (SIMS) and comparison with cation self-diffusion in corundum-structure oxides, Philos. Mag. **85**, 3643 (2005).

[6] S. Hallström, L. Höglund, and J. Ågren, Modeling of iron diffusion in the iron oxides magnetite and hematite with variable stoichiometry, Acta Mater. **59**, 53 (2011).

[7] A. Atkinson and R. I. Taylor, Diffusion of ^{55}Fe in Fe_2O_3 single crystals, J. Phys. Chem. Solids **46**, 469 (1985).

[8] G. Franceschi, M. Wagner, J. Hofinger, T. Krajňák, M. Schmid, U. Diebold, and M. Riva, Growth of $In_2O_3(111)$ thin films with optimized surfaces, Phys. Rev. Mater. **3**, 103403 (2019).

[9] M. Riva, G. Franceschi, M. Schmid, and U. Diebold, Epi-

taxial growth of complex oxide films: Role of surface reconstructions, Phys. Rev. Res. **1**, 033059 (2019).
[10] K. Reuter and M. Scheffler, Erratum: Composition, structure, and stability of RuO_2(110) as a function of oxygen pressure [Phys. Rev. B **65**, 035406 (2001)], Phys. Rev. B **75**, 049901 (2007).
[11] G. Ketteler, W. Weiss, W. Ranke, and R. Schlögl, Bulk and surface phases of iron oxides in an oxygen and water atmosphere at low pressure, Phys. Chem. Chem. Phys. **3**, 1114 (2001).
[12] A. G. Tamirat, J. Rick, A. A. Dubale, W.-N. Su, and B.-J. Hwang, Using hematite for photoelectrochemical water splitting: a review of current progress and challenges, Nanoscale Horiz. **1**, 243 (2016).